Experimental and theoretical evidence for the temperature-determined evolution of PAH functional groups

Experimental and Theoretical Evidence for the Temperature-determined Evolution of PAH Functional Groups

Peng Liu [a*], Bingjie Chen [a,c*], Zepeng Li [a], Anthony Bennett [a], Salim Sioud [b], Heinz Pitsch [c], S. Mani Sarathy [a], William L. Roberts [a]

a King Abdullah University of Science and Technology (KAUST), Clean Combustion Research Center, Thuwal 23955-6900, Saudi Arabia

b King Abdullah University of Science and Technology, Analytical Core Lab, Thuwal 23955-6900, Saudi Arabia

c Institute for Combustion Technology, RWTH Aachen University, Templergraben 64, Aachen 52062, Germany

Corresponding Authors:

Peng Liu
Clean Combustion Research Center, KAUST
Thuwal, 23955-6900, Saudi Arabia
E-mail: peng.liu.1@kaust.edu.sa

Bingjie Chen
Institute for Combustion Technology, RWTH Aachen University
Templergraben 64, 52062 Aachen, Germany
E-mail: b.chen@itv.rwth-aachen.de

Colloquium:

SOOT, NANOMATERIALS, AND LARGE MOLECULES

Word Count (Method 1):

The total word count (exclusive of title page, abstract) is: **5858** words

Word Count (Performed by automatic counting function in MS Word plus References/ Tables/ Equations/ Figures)

Abstract: **236** words, not included in word count
Main text: 3256 words
References: 542 words (29 references)
Tables: 0 words (0 tables)
Equations: 0 words (0 equations, single column)
Figures: 2060 words (6 figures with captions)

Figure	Column	Height/mm	Word Count
1	double	47.2	252
2	single	78.7	195
3	single	55.4	144
4	double	43.3	235
5	double	115.2	551
6	double	115.2	551
Captions			132

Supplemental Materials: Supplemental Material-1 and 2 are available.

Experimental and Theoretical Evidence for the Temperature-determined Evolution of PAH Functional Groups

Peng Liu [a*], Bingjie Chen [a,c*], Zepeng Li [a], Anthony Bennett [a], Salim Sioud [b], Heinz Pitsch [c], S. Mani Sarathy [a], William L. Roberts [a]

a King Abdullah University of Science and Technology (KAUST), Clean Combustion Research Center, Thuwal 23955-6900, Saudi Arabia

b King Abdullah University of Science and Technology, Analytical Core Lab, Thuwal 23955-6900, Saudi Arabia

c Institute for Combustion Technology, RWTH Aachen University, Templergraben 64, Aachen 52062, Germany

Abstract: Elucidating the chemical evolution of various functional groups in polycyclic aromatic hydrocarbons (PAH) and soot aids in understanding soot formation chemistry. In this work, the chemical evolution of various functional groups, including aromatic C-H, aliphatic C-H, C=O, C-OH and C-O-C bonds, was experimentally investigated online, rather than with offline diagnostics. Oxidation was performed in a jet-stirred reactor (JSR), fueled with benzene/C_2H_2/air/N_2 and benzene/phenol/C_2H_2/N_2 for a temperature range of 600-1400 K. Kinetic modelling, including *ab initio* quantum chemistry calculations, reaction rate coefficient calculations and JSR simulations, were conducted to interpret the experimental data and the evolutionary chemistry of the various functional groups. Results show that the formation of functional groups on PAH and oxygenated PAH (OPAH) are highly sensitive to temperature. Aliphatic C-H bonds survive mainly in the form of C-CH_2-C, C-CH_2-CH_2-C or C≡CH functional groups above 1200 K, and exist in the CH=CH_2 functional group below 1000 K. For the OPAH, the C-O-C functional group presents stronger thermal stability than C-OH and C=O functional groups. Simulation results indicate that

* Corresponding author: Emails: peng.liu.1@kaust.edu.sa (P. Liu), b.chen@itv.rwth-aachen.de (B. Chen)

HACA-like pathway (hydrogen abstraction carbon addition), in which C_2H_2 attacks the O atom, followed by cyclization and H-atom elimination reactions, qualitatively describe the formation of OPAH with the C-O-C functional group at different temperatures. The addition reaction involving PAH radical and C_2H_4 / C_2H_3 captures the evolution of PAH with the $CH=CH_2$ functional group, but fails to explain the formation of $C-CH_2-C$ and $C-CH_2-CH_2-C$ functional groups.

Key words: PAH, OPAH, functional groups, temperature dependence, soot.

1. Introduction

Soot produced from a controlled hydrocarbon combustion process can be a candidate material for rubber, printing inks, coatings, and battery cells [1]. The quality of soot is characterized by primary particle size, aggregate size, chemical composition and surface properties. The C/H ratio of incipient soot typically ranges from 1.4 to 2 (1.4 for phenanthrene, and 2 for coronene) [1, 2], and 10 to 20 for mature soot [3], indicating that the incipient soot is largely composed of moderate-sized polycyclic aromatic hydrocarbons (PAH), and that soot growth is a process of carbonization [4-7]. Consequently, the surface properties of soot are determined by various functional groups of PAH building blocks [2]. However, the chemical evolution of soot and PAH functional groups under combustion conditions is not well understood.

Using infrared spectroscopy, the chemical composition of dichloromethane-soluble PAH material sampled from sooting flame and soot was revealed by McKinnon *et al.*[8], Santamaria *et al.* [9], Ciajolo *et al.*[10, 11], and Cain *et al.* [12]. Their results showed that the aliphatic C-H content was greater than the aromatic C-H content for nascent particles in premixed sooting flames, and the main aliphatic constituents were alkylated aromatics [12]. The appreciable amount of aliphatic C-H bond in soot particle challenges the theory of PAH and soot formation, where soot growth is described mainly by a hydrogen abstraction carbon addition (HACA) mechanism [13, 14]. In the HACA mechanism, acetylene is the

dominant carbon species added to the active site of PAH and to the soot surface, because of its high concentration and high addition reaction rate with the C≡C triple bond [15-17]. Therefore, the formation of alkylated aromatics with an appreciable amount is not within the HACA framework. Furthermore, during analysis of soot composition sampled from laminar flames and diesel engines, oxygenated PAH (OPAH) functional groups, with C=O, C-O-C or C-OH bonds on soot, were experimentally identified by several research groups [18-20]. Using X ray photoelectron spectroscopy analysis, Johansson *et al.* [18] revealed that the content of the C-O-C functional group was higher than that of C=O and C-OH functional groups. It is notable that in previous studies [1, 2], offline particle diagnostic techniques were widely used for chemical composition analysis of soot. One issue in offline analysis is that the flame temperature profile changes greatly during the sampling process, which may alter the chemical evolution of the functional group. In the burner stabilized stagnation flame configuration, the sampling tube is inserted in the stagnation plate [12]. The temperature at seven (six) mm above the burner surface can drop from 1435 K (1601 K) to 393 K (1020 K) when the stagnation plate (sampling position) moves from 12 mm to 7 mm above the burner surface [21]. Investigating the temperature effect on chemical evolution of PAH functional groups using online measurements may provide a better understanding of PAH and soot formation.

This paper reports an experimental and theoretical study performed for the evolution of PAH functional groups in a temperature range of 600-1400 K. Experiments were conducted in a jet-stirred reactor (JSR), fueled with $C_6H_6/C_2H_2/air/N_2$ and $C_6H_6/C_6H_6O/C_2H_2/N_2$, with the products analyzed by a high-resolution mass spectrometer. It should be noted that the experimental data measured at 1400 K were presented in our previous paper [22], focusing on the role of OPAH in soot nucleation process. Here, the temperature-dependent chemical evolution of functional groups on PAH is investigated for the first time. Further, the discussion of aromatic C-H and aliphatic C-H functional groups is included. To better understand the

experimental results, density functional theory (DFT) and transition state theory (TST) calculations were performed to explore possible formation pathways for PAH detected with different functional groups.

2. Experimental and calculation methodology

2.1 JSR experiments

The experimental setup (Fig. 1) is similar to that reported in previous studies [23-25]; only a brief description is given here. The spherical reactor (volume 76 cm^3) includes fused silica to prevent surface reactions. Two sets of experiments were performed, fueled by $C_6H_6/C_2H_2/air/N_2$ and $C_6H_6/C_6H_6O/C_2H_2/N_2$. The mole fractions of C_6H_6, C_6H_6O, O_2, C_2H_2 and N_2 were 1000 ppm, 0, 1000 ppm, 1 % and 98.8 % in the $C_6H_6/C_2H_2/air/N_2$ experiment, and 500 ppm, 500 ppm, 0, 1 % and 98.9 % in the $C_6H_6/C_6H_6O/C_2H_2/N_2$ experiment, respectively. $C_6H_6/C_6H_6O/C_2H_2/N_2$ mixtures represent the main species involved in the growth of PAH and soot in sooting flames, where the typical concentrations of benzene and acetylene are around 500 ppm and 1 % respectively [26]. Here, phenol represents a partially oxidized product of benzene. Comparison experiments of $C_6H_6/C_2H_2/air/N_2$ with same amount of each element (C, H, O) were conducted, which contributes to distinguishing some OPAH isomers and reaction pathways. The vaporizer, designed and constructed at KAUST, was heated to 140 ºC to vaporize electronically-controlled liquid injections of C_6H_6 (Sigma Aldrich, purity > 99%) and C_6H_6O (Sigma Aldrich, purity > 98%); the vapor was then diluted by N_2 before introduction into the reactor. All gas flows were metered by MKS mass flow controllers, and the residence time in the reactor was fixed at 1.0 second. Temperature profiles, measured by a K-type thermocouple, showed good uniformity (gradient <3K/cm) inside the reactor, and the thermocouple monitored reactor temperatures at the reactor exit. The reactor temperature was scanned from 600 K to 1400 K with an interval of 100 K. A heated sampling probe was placed at the exit of the reactor, and the products were analyzed using an LTQ Velos Orbitrap mass spectrometer. The LTQ-Orbitrap mass analyzer was carefully calibrated following the manufacturer's guidelines. The Syagen's PhotoMate APPI source was the ionization source during

experiments. Capillary temperature under the APPI source mode was maintained at a constant 350˚C during all experiments, and the source vaporizer temperature was set to 450˚C. The ionization energy of the krypton lamp was fixed at 10.6 eV, high enough to ionize all investigated PAH molecules. The mass scan range (*m/z*) was set to 70–300. Accurate masses were meticulously obtained at a high resolving power ($m/\Delta m \approx 100000$), sensitivity (1-5 ppm) and mass accuracy (< 5 ppm). In this way, the chemical formula could be unambiguously assigned to the interested signal. Furthermore, the linear ion trap confined one specific molecular ion in a narrow mass range ($\Delta m/z < 0.001$), isolated and fragmented it to identify the functional groups. Details of trapped species fragmentation pattern are presented in Supplementary Material 2. The detection limit was estimated to be 1 ppm, and the overall error was estimated within 20%, which is too small to influence any conclusions [24].

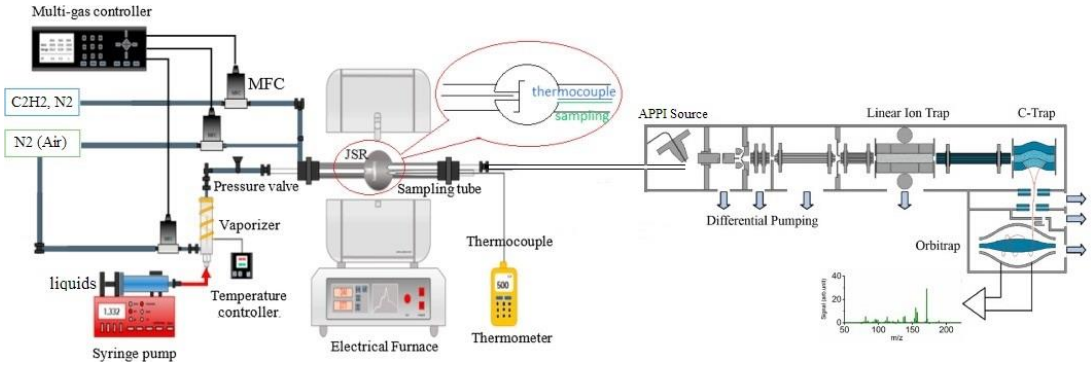

Figure 1: Experimental setup for JSR experiments [23, 25].

2.2 Kinetic modelling

PAH containing oxygen atoms or aliphatic C-H bonds were detected and identified experimentally, but their formation pathways and kinetic parameters remain unclear. In this study, the potential formation pathways were explored at the DFT B3LYP/6-311+G(d,p) level. The energies of each optimized structure were further refined using a CCSD(T)/cc-pvdz method. Transition states were checked by intrinsic reaction coordinate (IRC) calculations. All quantum chemistry calculations were conducted using the Gaussian 09 software package, version D.01 [27]. Based on frequencies, energy barriers, and rotation

constant information, the reaction rate coefficients of elementary reactions were evaluated using TST, which considered the Eckart tunneling correction and reaction pathway degeneracy. These new reactions were merged into a detailed PAH mechanism [22] to predict the concentrations of various PAH in a perfectly stirred reactor using Chemkin Pro software [28]. Other PAH formation reaction pathways involving additional species like C_5H_5, C_4H_5, C_4H_4, C_3H_4, C_3H_3, C_2H_3, C_2H_2, C_2H, CH_3, and CH_2 are included in the current PAH mechanism. It should be noted that not all possible and potentially important pathways leading to the formation of PAH and OPAH are in the model. The aim of this paper is to fill the gap. The input parameters for the perfectly stirred reactor (including mole fraction of reactants, reaction temperature, and residence time) were identical to those in the experiments.

3. Results and discussions

The mass spectra of $C_6H_6/C_2H_2/air/N_2$ and $C_6H_6/C_6H_6O/C_2H_2/N_2$ reaction products were recorded at a temperature interval of 100 K in the experiments. To show the evolution of various functional group with temperature, only the spectra at 600 K, 800 K, 1000 K, 1200 K and 1400 K are shown in Fig. 2. It should be noted that signal intensity data, recorded at every temperature point, are used in the following analysis. Due to the space limitation, we focus on a discussion of PAH functional groups discussion for the $C_6H_6/C_6H_6O/C_2H_2/N_2$ case. The results from the $C_6H_6/C_2H_2/air/N_2$ case are presented in the Supplementary Material 1 (SM1). Molar concentrations could not be determined from the experimental data because ionization efficiency for all possible molecules at a particular mass-to-charge ratio are unknown.

Generally, the reaction products of $C_6H_6/C_6H_6O/C_2H_2/N_2$ and $C_6H_6/C_2H_2/air/N_2$ present two main features along the reaction temperature zone. Only oxygenated aromatic hydrocarbons signals (C_6H_6O, C_7H_4O, and C_8H_6O) are observed, with a relatively weak intensity in the low temperature region (600-800 K), as shown in Fig. 2 and Fig. S1. In the temperature range of 900-1400 K, signals of aromatic hydrocarbons and oxygenated aromatic hydrocarbons emerge simultaneously, and the signal intensity of

large aromatic hydrocarbons ($C_{12}H_8$ and $C_{16}H_{14}$) increases at higher temperatures, while the signal intensity of small aromatic hydrocarbons (C_6H_6 and C_8H_6) displays the opposite trend. The growth of larger PAH and OPAH molecules is highly sensitive to the radical concentrations and the corresponding growth reaction rate, because the activation of the close-shell PAH and OPAH molecules by radical species is the first step in PAH and OPAH growth pathway, followed by the addition reaction of carbon species. In this study, the simulated peak mole fraction of H atom for $C_6H_6/C_2H_2/air/N_2$ experiment is 6.08×10^{-11} at 600 K and becomes 4.86×10^{-7} at 1400 K. The calculated reaction coefficients of C_2H_2+phenyl reaction is 1.1×10^8 $cm^3/mol/s$ at 600 K and 4.5×10^{11} $cm^3/mol/s$ at 1400 K[13]. Therefore, the observed phenomenon may be explained by the temperature-dependent radical concentration and growth reaction rate of PAH and OPAH. In the following section, signal intensity trends along different temperatures are discussed for OPAH and PAH, focusing on the evolution of C=O, C-OH, C-O-C, aromatic C-H and aliphatic C-H bonds.

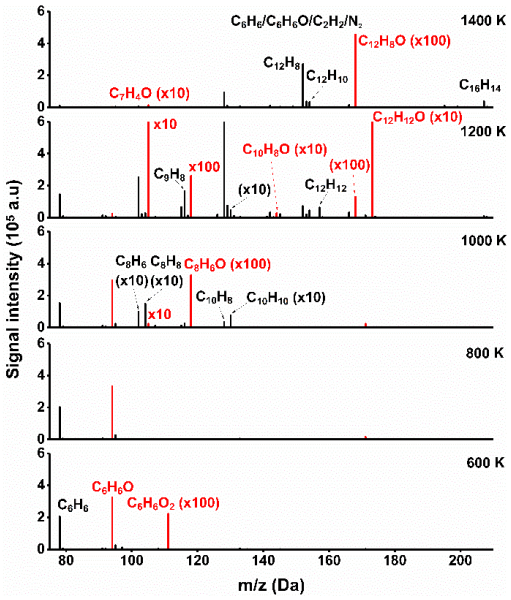

Figure 2: Mass spectra of benzene/phenol/acetylene/nitrogen reaction products in JSR at different temperatures. Red lines indicate OPAH; black lines are PAH.

3.1 OPAH with C-OH, C=O and C-O-C functional groups

The functional groups for measured C_6H_6O (C-OH), C_7H_4O (C=O), C_8H_6O (C-O-C), and $C_{12}H_8O$ (C-O-C) are discussed next. To identify functional groups, the species involved were trapped and fragmented at relatively high energy. Based on fragment information and calculated concentration ratios among isomers for selected signals, the most probable structure was determined. For example, the C_8H_6O signal could be emitted from benzofuran, ethynyloxybenzene, and 3-hydroxyphenylacetylene (see structure A, B, C in Fig. 3) in the $C_6H_6/C_6H_6O/C_2H_2/N_2$ system. The $C_xH_{y-2}O_{z-1}$ signal would be observed if the $C_xH_yO_z$ structure contained the C-OH functional group, because of the release of the H_2O fragment. Therefore, 3-hydroxyphenylacetylene is excluded, since the C_8H_4 signal is not observed in C_8H_6O fragmentation mass spectra in Fig. 3. The formation pathways of benzofuran and ethynyloxybenzene were considered via the reaction of $C_6H_5O+C_2H_2$. The corresponding potential energy surfaces are shown in Fig. 4, and the kinetic rates of this reaction are provided in Table S1 in the SM1. The simulated results indicate that benzofuran should be the dominant cause for the C_8H_6O signal, since the simulated mole fraction of benzofuran is higher than that of ethynyloxybenzene by at least four orders of magnitude in all investigated conditions. Fragment information for all the species involved is presented in the SM1.

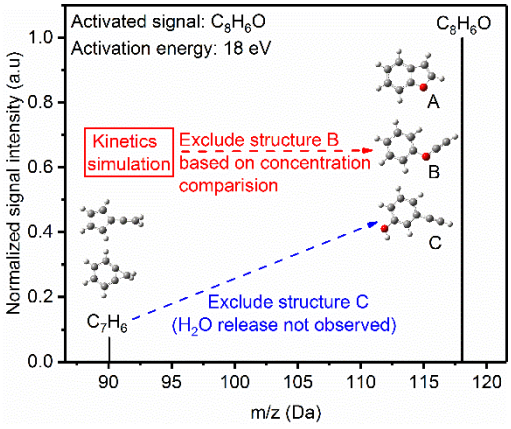

Figure 3: Fragmentation mass spectra of experimentally "trapped" C_8H_6O. The possible species benzofuran (A), ethynyloxybenzene (B), and 3-hydroxyphenylacetylene (C) were considered for the C_8H_6O signal.

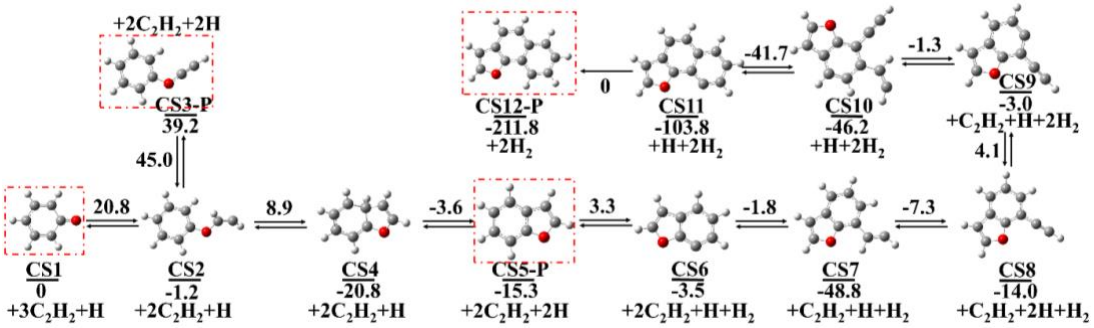

Figure 4. The formation pathway of C_8H_6O and $C_{12}H_8O$ from C_6H_5O. Energy unit is kcal/mol.

The measured signal-vs.-temperature profiles for C_6H_6O, C_7H_4O, C_8H_6O, and $C_{12}H_8O$ are presented in Fig. 5. The rapid decrease for higher temperatures of C_6H_6O is observed in the $C_6H_6/C_6H_6O/C_2H_2/N_2$ experiment in the 1000-1200 K temperature range, corresponding to the rapid formation of C_7H_4O, C_8H_6O and $C_{12}H_{12}O$ species (Fig. 5b and 5c); therefore, C_6H_6O could be the precursor of these species. The formation of $C_{12}H_8O$ (Fig. 5d) is very different from C_6H_6O, C_7H_4O, C_8H_6O and $C_{12}H_{12}O$. The signal appears up to 1200 K, and a decreasing trend is not observed. Two production pathways, including $C_{10}H_7O+C_2H_2 \rightarrow C_{12}H_8O+H$ [22] and $C_8H_6O+H \rightarrow C_8H_5O\ (+C_2H_2) \rightarrow C_{10}H_7O\ (+C_2H_2) \rightarrow C_{12}H_8O+H$, were considered in the PAH mechanism (Fig. 4). The simulation results in the case for 1400 K in $C_6H_6/C_2H_2/air/N_2$ indicate that the latter pathway dominates $C_{12}H_8O$ production, and the contribution to yield is 75.2 % (Fig. S9 in SM1). So, it is understandable that the signal of $C_{12}H_8O$ increases rapidly at the temperature where the signal of C_8H_6O rapidly decreases.

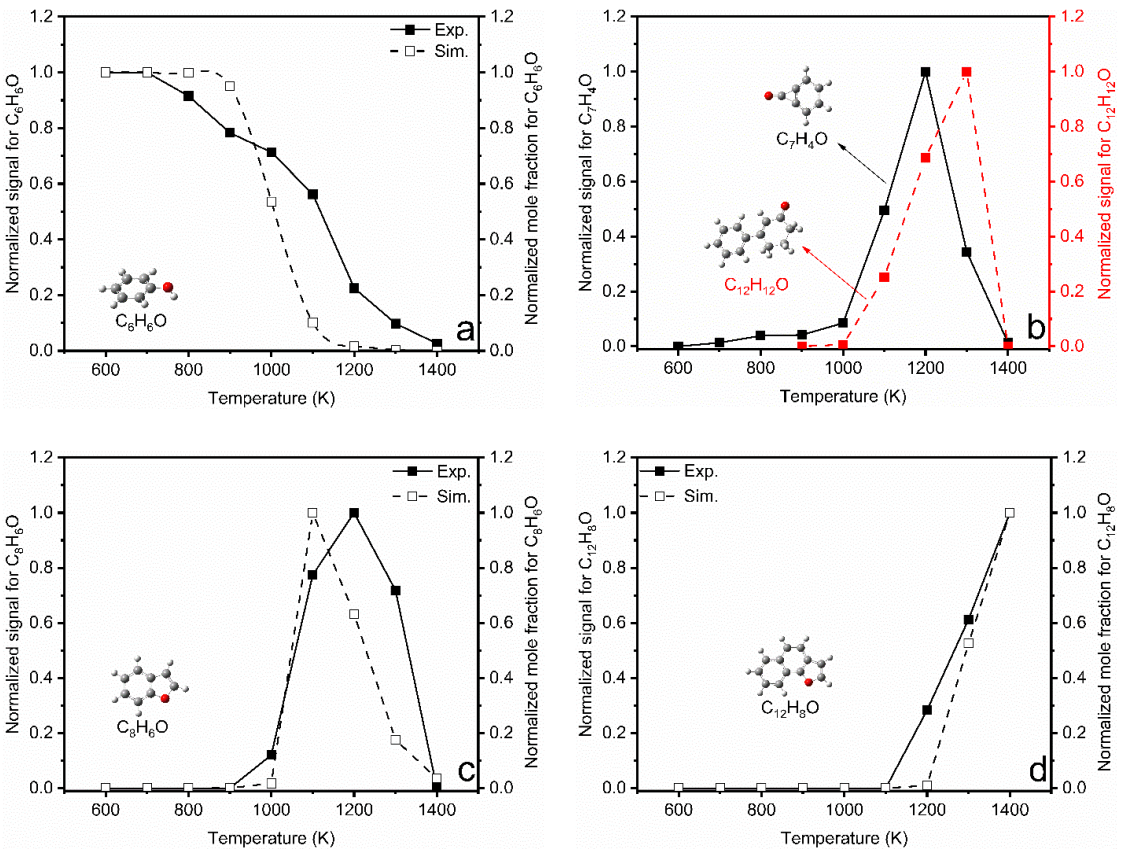

Figure 5: Measured and simulated concentration evolution trends for various OPAH at different temperatures in $C_6H_6/C_6H_6O/C_2H_2/N_2$ experiments. Most likely structures are indicated. The scaling factors for C_6H_6O, C_8H_6O, and $C_{12}H_8O$ species are $2.0x10^3$, $3.6x10^7$, and $7.5x10^9$, respectively.

The simulated mole fractions of interested PAH and OPAH were presented in Table S2 and S3 in SM1. Here, simulated species mole fractions were normalized by the maximum value to better compare with the experimental data. Generally, the trend of simulated C_6H_6O, C_8H_6O and $C_{12}H_8O$ concentration profiles match well with the measured profiles, as shown in Fig. 5. This means that the proposed pathway C_6H_6O $(+H+C_2H_2) \rightarrow C_8H_6O$ $(+H+2C_2H_2) \rightarrow C_{12}H_8O$ as shown in Fig. 4 qualitatively predicts the formation of OPAH, like benzofuran. Some disagreement between experimental and predicted results are observed in $C_6H_6/C_2H_2/air/N_2$ case. It is noted that the predicted inflection point of the C_8H_6O curve (800 K) in $C_6H_6/C_2H_2/air/N_2$ case is lower than the measured point (1200 K) by 400 K as shown in Fig. S2-c, which may result from the overly fast conversion of C_6H_6O to C_8H_6O at low temperatures. Indeed, C_6H_6O is

under-predicted in $C_6H_6/C_2H_2/air/N_2$ case in the temperature range of 600-1000 K, as shown in Fig. S2-a. Therefore, further development of OPAH model is needed in future work.

Based on the above discussion, it can be concluded that the formation of C-OH, C=O and C-O-C functional groups on PAH and soot has significant temperature sensitivity. Specifically, the C-OH functional group is the preferred product at temperatures below 1100 K due to the relative energy barrier in oxidation reaction, and the C=O functional group is mainly formed at moderated temperatures (1100-1300 K). The C-O-C functional group is the only one that survives above 1400 K.

3.2 PAH with aliphatic C-H bond and aromatic C-H bond

The signals of C_8H_8, C_9H_8, $C_{10}H_{10}$, $C_{12}H_{10}$, $C_{12}H_{12}$, $C_{13}H_{10}$, and $C_{16}H_{14}$ were detected in both $C_6H_6/C_6H_6O/C_2H_2/N_2$ and $C_6H_6/C_2H_2/air/N_2$ experiments, in which the H radical had low mole fractions below 1400 K (less than 5×10^{-7} in simulations). These PAH species contain aliphatic C-H bonds. The functional group identification strategy for the signals of involved PAH with the aliphatic C-H bond is the same as for OPAH. Here, the signal ratio of C_8H_8/C_8H_6, $C_{10}H_{10}/C_{10}H_8$, and $C_{12}H_{10}/C_{12}H_8$ pairs are discussed, to reveal the evolution trend between the ratio of aliphatic C-H and aromatic C-H functional groups on nascent soot [12]. As shown in Fig. 6, the carbonization process causes the signal ratios of C_8H_8/C_8H_6, $C_{10}H_{10}/C_{10}H_8$, and $C_{12}H_{10}/C_{12}H_8$ to be significantly sensitive to temperature. The evolution of C_8H_8/C_8H_6, $C_{10}H_{10}/C_{10}H_8$, and $C_{12}H_{10}/C_{12}H_8$ signal ratio profiles is similar, but the ratio values are different. The signal ratios of C_8H_8/C_8H_6, $C_{10}H_{10}/C_{10}H_8$, and $C_{12}H_{10}/C_{12}H_8$ are 12.9 (0.09), 0.23 (0), and 3.0 (0.42) at 900 K (1400 K), respectively, in the $C_6H_6/C_2H_2/air/N_2$ experiment, and are 1.97 (0), 0.06 (0), 1.0 (0.12) at 1000 K (1400 K) in the $C_6H_6/C_6H_6O/C_2H_2/N_2$ experiment. These results indicate that the aliphatic C-H bond exists mainly in the form of C_2H_3 substitution (like styrene, C_8H_8) at temperatures below 900 K, and in the alkylated aromatic with a five-member ring (like acenaphthene, $C_{12}H_{10}$) and C_2H

substitution (like phenylacetylene, C_8H_6) at temperatures above 1400 K. On the other hand, the measured profiles of signal ratio are close between $C_6H_6/C_6H_6O/C_2H_2/N_2$ and $C_6H_6/C_2H_2/air/N_2$ experiments, as shown in Fig. S3-a-c. This means that the signal ratios of the PAH with aliphatic C-H and aromatic C-H functional groups are not sensitive to the existence of oxygen atom in phenol. Addition reactions of PAH + C_2H_3 → PAH-C_2H_3 + H and PAH radical + C_2H_4 → PAH-C_2H_3 + H were considered in this study to form C_8H_8, $C_{10}H_{10}$, and $C_{12}H_{10}$. This pathway is recommended by Shukla *et al*.[29], based on the observed sequence of mass peaks with intervals of 26 in ethylene pyrolysis experiment at moderate temperature (~1300K). The formation pathways of both $C_{10}H_{10}$ isomers (dialin and 1,3-diethenylbenzene) were considered in the model (see Fig. S8-S9 in the supplementary material). The simulated concentration of 1,3-diethenylbenzene is much higher than that of dialin by a factor of 100. Therefore, 1,3-diethenylbenzene should be the main contributor to the $C_{10}H_{10}$ signal in this study. As shown in Fig. 6a, the main features of the signal ratio profiles of C_8H_8/C_8H_6 are well captured by the current PAH mechanism, but not for $C_{10}H_{10}/C_{10}H_8$ at temperatures below 1000 K in $C_6H_6/C_6H_6O/C_2H_2/N_2$ experiment. The high-temperature chemistry of $H_2/CO/C_1$-C_4 compounds from USCII was used in this study, which may be the reason for this disagreement at low temperature. It is worthy mentioning that $C_{10}H_8$ (naphthalene) is dominantly formed from the recombination reaction of two cyclopentadienides and the growth reaction involving phenylacetylene, instead of the dehydrogenation reaction ($C_{10}H_{10}$ → $C_{10}H_8$ + H_2) based on the reaction pathway analysis. The predicted mole fraction of $C_{12}H_{10}$ (acenaphthene) is lower than 10^{-10}, so other pathways (beyond 1-naphthyl radical + C_2H_4 and naphthalene + C_2H_3 reactions) should be explored to account for the acenaphthene formation. For this reason, the simulated signal ratio profiles of $C_{12}H_{10}/C_{12}H_8$ are not presented here.

Considering that the flame temperature is generally higher than 1400 K in soot formation region, it can be deduced that aliphatic C-H bonds on PAH and soot are likely to exist in the form of C-CH_2-C, and C≡CH functional groups.

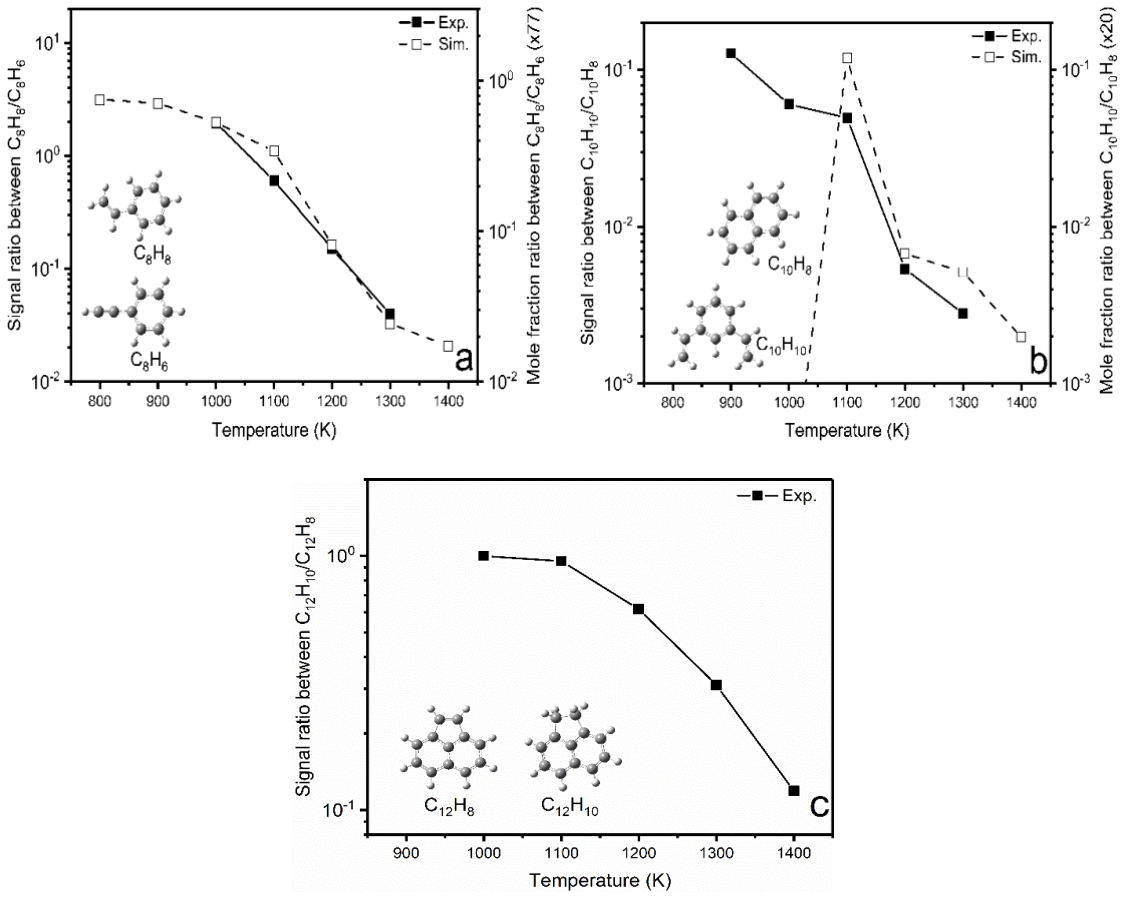

Figure 6: Measured and simulated concentration ratio trends for PAH containing aliphatic C-H and aromatic C-H functional groups at different temperatures. Most likely structures are indicated.

4. Conclusions

The evolution of different functional groups, as a function of temperature, was experimentally studied in a jet-stirred reactor (JSR) fueled with $C_6H_6/C_2H_2/air/N_2$ and $C_6H_6/C_6H_6O/C_2H_2/N_2$. Kinetic model calculations, including reaction pathway exploration, reaction rate coefficient evaluations and JSR simulation, were conducted. The following conclusions were noted:

1. Joint consideration of the trapped molecule fragment spectrum, and predicted concentration ratios between isomers, was proven to effectively resolve isomeric structures for the involved species.

2. Formation of PAH and OPAH was highly sensitive to temperature. With increased temperature, the signals of large PAH increased and signals of small PAH decreased, which can be explained by kinetic effect. Various PAH with aliphatic C-H bond were detected and measured. The aliphatic C-H bonds on PAH and soot were likely to exist in the form of C-CH_2-C and C≡CH functional groups during soot nucleation (T > 1200 K), and the formation of CH=CH_2 functional group was favored at temperatures below 1000 K. The formation of OPAH with C-O-C functional group was enhanced at temperatures beyond 1200 K, while signals of OPAH with C-OH and C=O functional groups decreased rapidly.

3. The HACA-like pathway (C_2H_2 attacks the O atom, followed by the cyclization and H elimination reactions) and the addition reactions of the PAH radical + C_2H_4 and PAH + C_2H_3 were proposed to describe the formation of the interested species. Comparisons between detected and predicted results indicated that the HACA-like reactions qualitatively described the formation of OPAH with the C-O-C functional group. The addition reactions of the PAH radical + C_2H_4 and PAH + C_2H_3 captured the evolutionary trend of PAH with CH=CH_2 functional groups, but failed to explain the formation of C-CH_2-C functional group. More work is required in the future to understand the formation mechanism of PAH with C-CH_2-C functional groups.

List of Supplemental Material

Supplementary Material-1:

Fig. S1. Mass spectra of benzene/acetylene/oxygen/nitrogen reaction products in JSR at different temperatures. Red lines indicate OPAH; black lines are PAH.

Fig. S2. Measured and simulated concentration evolution trends for various OPAH at different temperatures. Most likely structures are indicated.

Fig. S3. Measured and simulated concentration ratio trends for PAH containing aliphatic C-H and aromatic C-H functional groups at different temperatures. Most likely structures are indicated.

Fig. S4. Fragmentation mass spectra of experimentally "trapped" C_7H_4O.

Fig. S5. Fragmentation mass spectra of experimentally "trapped" $C_{10}H_8O$.

Fig. S6. Fragmentation mass spectra of experimentally "trapped" $C_{12}H_{10}$.

Fig. S7. Fragmentation mass spectra of experimentally "trapped" $C_{12}H_{12}O$.

Fig. S8. The possible decomposition pathway of $C_{12}H_{12}O$ fragmentation.

Fig. S9. The simulated mole fraction of $C_{12}H_8O$ at 1400 K in a 0-D batch reactor fueled with $C_6H_6/C_2H_2/air/N_2$. There are two pathways ($C_{10}H_7O+C_2H_2 \rightarrow C_{12}H_8O+H$ and $C_8H_6O+H \rightarrow C_8H_5O$ $(+C_2H_2) \rightarrow C_{10}H_7O$ $(+C_2H_2) \rightarrow C_{12}H_8O+H$) considered in the PAH mechanism. The results indicate that the later pathway is the dominant pathway leading to the formation of $C_{12}H_8O$ (contribution is 75.2 %).

Fig. S10. The formation pathway of C_8H_8 and $C_{10}H_{10}$ from C_6H_6. Energy unit is kcal/mol.

Fig. S11. The formation pathway of $C_{10}H_{10}$ from C_8H_5 and $C_{12}H_{10}$ from $C_{10}H_8$. Energy unit is kcal/mol.

Table S1. Reaction rate parameters in the form of $A \cdot T^n \cdot \exp(-E/(RT))$, units are s^{-1}, $cm^3mol^{-1}s^{-1}$ and kcal.

Table S2. The simulated PAH and OPAH mole fraction in $C_6H_6/C_2H_2/air/N_2$ experiments. The maximum value is highlighted with yellow color.

Table S3. The simulated PAH and OPAH mole fraction in $C_6H_6/C_6H_6O/C_2H_2/N_2$ experiments. The maximum value is highlighted with yellow color.

Table S4. Energies, expectation values of S^2 operator (projected values are in parentheses), vibrational frequencies, rotational constants, external symmetry number, optical isomers, electronic ground state, Lennard-Jones parameters for all optimized structures at DFT/B3LYP/6-311+G(d,p) level in this work.

Table S5. The Cartesian coordinates of the optimized structures at DFT/B3LYP/6-311+G(d,p) level.

Supplementary Material-2:

Part 1: Detailed description on Atmospheric Pressure Photo Ionization (APPI)

Part 2: Detailed description on LTQ Orbitrap (Linear ion Trap & Orbitrap analyzer)

Acknowledgments

The work at King Abdullah University of Science and Technology (KAUST) was supported by the KAUST Clean Fuels Consortium (KCFC) and its member companies. Calculations were run with the support of KAUST Supercomputing Lab (Shaheen & Ibex). BC and HP gratefully acknowledge financial support by the Deutsch Forschungsgemeinschaft within the framework of the collaborative research center SFB/Transregio 129 “Oxyflame”.

References:

[1] H. Wang, Formation of nascent soot and other condensed-phase materials in flames, Proc. Combust. Inst. 33 (2011) 41-67.
[2] H.A. Michelsen, Probing soot formation, chemical and physical evolution, and oxidation: A review of in situ diagnostic techniques and needs, Proc. Combust. Inst. 36 (2017) 717-735.
[3] C. Russo, M. Alfè, J.-N. Rouzaud, F. Stanzione, A. Tregrossi, A. Ciajolo, Probing structures of soot formed in premixed flames of methane, ethylene and benzene, Proc. Combust. Inst. 34 (2013) 1885-1892.
[4] F. Schulz, M. Commodo, K. Kaiser, G. De Falco, P. Minutolo, G. Meyer, A. D`Anna, L. Gross, Insights into incipient soot formation by atomic force microscopy, Proc. Combust. Inst. 37 (2019) 885-892.
[5] P. Liu, Z. Li, W.L. Roberts, The growth of PAHs and soot in the post-flame region, Proc. Combust. Inst. 37 (2019) 977-984.

[6] M. Frenklach, Z. Liu, R.I. Singh, G.R. Galimova, V.N. Azyazov, A.M. Mebel, Detailed, sterically-resolved modeling of soot oxidation: Role of O atoms, interplay with particle nanostructure, and emergence of inner particle burning, Combust. Flame 188 (2018) 284-306.
[7] Y. Bouvier, C. Mihesan, M. Ziskind, E. Therssen, C. Focsa, J.F. Pauwels, P. Desgroux, Molecular species adsorbed on soot particles issued from low sooting methane and acetylene laminar flames: A laser-based experiment, Proc. Combust. Inst. 31 (2007) 841-849.
[8] J.T. McKinnon, E. Meyer, J.B. Howard, Infrared analysis of flame-generated PAH samples, Combust. Flame 105 (1996) 161-166.
[9] A. Santamaría, F. Mondragón, A. Molina, N.D. Marsh, E.G. Eddings, A.F. Sarofim, FT-IR and 1H NMR characterization of the products of an ethylene inverse diffusion flame, Combust. Flame 146 (2006) 52-62.
[10] A. Ciajolo, A. D'Anna, R. Barbella, A. Tregrossi, A. Violi, The effect of temperature on soot inception in premixed ethylene flames, Proc. Combust. Inst. 26 (1996) 2327-2333.
[11] C. Russo, F. Stanzione, A. Tregrossi, A. Ciajolo, Infrared spectroscopy of some carbon-based materials relevant in combustion: Qualitative and quantitative analysis of hydrogen, Carbon 74 (2014) 127-138.
[12] J.P. Cain, J. Camacho, D.J. Phares, H. Wang, A. Laskin, Evidence of aliphatics in nascent soot particles in premixed ethylene flames, Proc. Combust. Inst. 33 (2011) 533-540.
[13] P. Liu, Z. Li, A. Bennett, H. Lin, S.M. Sarathy, W.L. Roberts, The site effect on PAHs formation in HACA-based mass growth process, Combust. Flame 199 (2019) 54-68.
[14] M. Frenklach, R.I. Singh, A.M. Mebel, On the low-temperature limit of HACA, Proc. Combust. Inst. 37 (2019) 969-976.
[15] Y. Wang, S.H. Chung, Soot formation in laminar counterflow flames, Prog. Energy Combust. Sci. 74 (2019) 152-238.
[16] J. Appel, H. Bockhorn, M. Frenklach, Kinetic modeling of soot formation with detailed chemistry and physics: laminar premixed flames of C2 hydrocarbons, Combust. Flame 121 (2000) 122-136.
[17] P. Liu, H. Lin, Y. Yang, C. Shao, B. Guan, Z. Huang, Investigating the Role of CH2 Radicals in the HACA Mechanism, J. Phys. Chem. A 119 (2015) 3261-3268.
[18] K.O. Johansson, T. Dillstrom, M. Monti, F. El Gabaly, M.F. Campbell, P.E. Schrader, D.M. Popolan-Vaida, N.K. Richards-Henderson, K.R. Wilson, A. Violi, H.A. Michelsen, Formation and emission of large furans and oxygenated hydrocarbons from flames, Proc. Nat. Acad. Sci. 113 (2016) 8374-8379.
[19] X. Li, Y. Zheng, C. Guan, C.S. Cheung, Z. Huang, Effect of biodiesel on PAH, OPAH, and NPAH emissions from a direct injection diesel engine, Environ. Sci. Pollut. Res. 25 (2018) 34131-34138.
[20] R. Nyström, I. Sadiktsis, T.M. Ahmed, R. Westerholm, J.H. Koegler, A. Blomberg, T. Sandström, C. Boman, Physical and chemical properties of RME biodiesel exhaust particles without engine modifications, Fuel 186 (2016) 261-269.
[21] C. Gu, H. Lin, J. Camacho, B. Lin, C. Shao, R. Li, H. Gu, B. Guan, Z. Huang, H. Wang, Particle size distribution of nascent soot in lightly and heavily sooting premixed ethylene flames, Combust. Flame 165 (2016) 177-187.
[22] P. Liu, B. Chen, Z. Li, A. Bennett, S. Sioud, S.M. Sarathy, W.L. Roberts, Evolution of oxygenated polycyclic aromatic hydrocarbon chemistry at flame temperatures, Combust. Flame 209 (2019) 441-451.
[23] Z. Wang, B. Chen, K. Moshammer, D.M. Popolan-Vaida, S. Sioud, V.S.B. Shankar, D. Vuilleumier, T. Tao, L. Ruwe, E. Bräuer, N. Hansen, P. Dagaut, K. Kohse-Höinghaus, M.A. Raji, S.M. Sarathy, n-Heptane cool flame chemistry: Unraveling intermediate species measured in a stirred reactor and motored engine, Combust. Flame 187 (2018) 199-216.
[24] Z. Wang, D.M. Popolan-Vaida, B. Chen, K. Moshammer, S.Y. Mohamed, H. Wang, S. Sioud, M.A. Raji, K. Kohse-Höinghaus, N. Hansen, P. Dagaut, S.R. Leone, S.M. Sarathy, Unraveling the

structure and chemical mechanisms of highly oxygenated intermediates in oxidation of organic compounds, Proc. Natl. Acad. Sci., (2017) 201707564.
[25] B. Chen, Z. Wang, J.-Y. Wang, H. Wang, C. Togbé, P.E.Á. Alonso, M. Almalki, M. Mehl, W.J. Pitz, S.W. Wagnon, K. Zhang, G. Kukkadapu, P. Dagaut, S. Mani Sarathy, Exploring gasoline oxidation chemistry in jet stirred reactors, Fuel 236 (2019) 1282-1292.
[26] Cheméo, available at <https://www.chemeo.com/cid/25-137-2/Ovalene>.
[27] M.J. Frisch, G.W. Trucks, H.B. Schlegel, G.E. Scuseria, M.A. Robb, J.R. Cheeseman, G. Scalmani, V. Barone, B. Mennucci, G.A. Petersson, et al., Gaussian 09 revision D.01; Gaussian, Inc.: Wallingford, CT,, (2013).
[28] R. Kee, F. Rupley, J. Miller, *CHEMKIN-PRO 15112, Reaction Design, San Diego, CA*, 2011.
[29] B. Shukla, M. Koshi, A novel route for PAH growth in HACA based mechanisms, Combust. Flame 159 (2012) 3589-3596.

List of Figure Captions

(Color figures in electronic version only)

Figure 2: Experimental setup for JSR experiments [23, 25].

Figure 2: Mass spectra of a) benzene/acetylene/air/nitrogen and b) benzene/phenol/acetylene/nitrogen reaction products in JSR at different temperatures. Red lines indicate OPAH; black lines are PAH.

Figure 3: Fragmentation mass spectra of experimentally "trapped" C_8H_6O. The possible species benzofuran (A), ethynyloxybenzene (B), and 3-hydroxyphenylacetylene (C) were considered for C_8H_6O signal.

Figure 4. The formation pathway of C_8H_6O and $C_{12}H_8O$ from C_6H_5O. Energy unit is kcal/mol.

Figure 5: Measured and simulated concentration evolution trends for various OPAH at different temperatures in $C_6H_6/C_6H_6O/C_2H_2/N_2$ experiment. Most likely structures are indicated. The scaling factors for C_6H_6O, C_8H_6O, and $C_{12}H_8O$ species are $2.0x10^3$, $3.6x10^7$, and $7.5x10^9$, respectively.

Figure 6: Measured and simulated concentration ratio trends for PAH containing aliphatic C-H and aromatic C-H functional groups at different temperatures. Most likely structures are indicated.